Received: 3 August 2019 | Revised: 20 February 2020 | Accepted: 24 February 2020

DOI: 10.1002/jbm.a.36913

Society For Biomaterials | WILEY

ORIGINAL ARTICLE

Modeling the upper airway: A precursor to personalized surgical interventions for the treatment of sleep apnea

Lachlan Hingley[1] | Ali Jeiranikhameneh[2] | Stephen Beirne[2] | Gregory Peoples[1] | Andrew Jones[1,3] | Sepidar Sayyar[2] | Peter Eastwood[4,5] | Richard Lewis[6] | Gordon Wallace[2] | Stuart G. MacKay[1,3,7]

[1]School of Medicine, University of Wollongong, Wollongong, New South Wales, Australia

[2]Australian Institute of Innovative Materials, University of Wollongong, Wollongong, New South Wales, Australia

[3]Illawarra Shoalhaven Local Health District, Wollongong, New South Wales, Australia

[4]Centre for Sleep Science, School of Human Sciences, University of Western Australia, Perth, Western Australia, Australia

[5]West Australian Sleep Disorders Research Institute, Sir Charles Gardiner Hospital, Perth, Western Australia, Australia

[6]Department of Otolaryngology Head & Neck Surgery, Royal Perth Hospital, Perth, Western Australia, Australia

[7]Illawarra ENT Head and Neck Clinic, Wollongong, New South Wales, Australia

Correspondence
Stuart G. MacKay, Illawarra ENT Head and Neck Clinic, 8-10 Victoria Street, Wollongong, NSW 2500, Australia.
Email: sgmackay@ozemail.com.au

Funding information
Garnett Passe and Rodney Williams Memorial Foundation, Grant/Award Number: Conjoint Grant 2016-2018

Abstract

An accurate benchtop model was developed to mimic the different forms of human upper airway collapse in adult sleep apnea patients. This was done via modeling the airway through digital imaging. Airway representative models were then produced in two steps via a customized pneumatic extrusion 3D printing system. This allowed the pressure of collapse and planes of collapse to be manipulated to accurately represent those seen in sleep apnea patients. The pressure flow relationships of the collapsible airways were then studied by inserting the collapsible airways into a module that allowed the chamber pressure (P_c) around the airways to be increased in order to cause collapse. Airways collapsed at physiologically relevant pressures (5.32–9.58 cmH_2O). Nickel and iron magnetic polymers were then printed into the airway in order to investigate the altering of the airway collapse. The introduction of the nickel and iron magnetic polymers increased the pressure of collapse substantially (7.38–17.51 cmH_2O). Finally, the force produced by the interaction of the magnetic polymer and the magnetic module was studied by measuring a sample of the magnetic airways. The peak force in (48.59–163.34 cN) and the distance over which the forces initially registered (6.8–9.7 mm) were measured using a force transducer. This data set may be used to inform future treatment of sleep apnea, specifically the production of an implantable polymer for surgical intervention.

KEYWORDS

airway modeling, obstructive sleep apnea, personalized, sleep surgery, smart polymer

1 | INTRODUCTION

The human upper airway is a dynamic, nonlinear, multifunctional structure with defined and well-studied biomechanical properties (Bilston & Gandevia, 2013). These properties, such as airway resistance and patency, result from active and passive components working to balance pressure in the airway with dilatory forces of the surrounding soft tissues (Huang, Malhotra, & White, 2005).

In some individuals, passive components like size, shape, and composition, predispose the airway to collapse, which can lead to obstructive sleep apnea (OSA). OSA in adults is a chronic, potentially progressive condition characterized by repetitive nocturnal upper airway closure or narrowing. Negative cardiovascular, metabolic, and quality of life outcomes are well established with prevalence in men from 4 to 24% and women from 2 to 9% (Young et al., 1993). Current treatments are limited by tolerance, adherence, and cost, and a considerable volume of patients remain untreated, leading to significant health and economic burden (Hillman et al., 2018).

Due to the complex personalized nature of the airway, establishing a unifying pathophysiology of OSA is difficult. Furthermore,

apart from perhaps the rodent model (Brennick et al., 2009; Brennick, Pickup, Cater, & Kuna, 2006), investigators are hampered by the lack of suitable animal models, which limits the development of novel treatment modalities. Previous benchtop physical models have been used to characterize the geometrical characteristics of the upper airway in OSA. One example is the "floppy" tube Starling resistor model that relates critical airflow (Pcrit), lumen geometry, and longitudinal wall strain to passive pharyngeal airway function in humans (Amatoury, Kairaitis, Wheatley, Bilston, & Amis, 2010). Using a Penrose drain contained within an enclosed chamber, the authors defined rate of airflow through the tube as influenced by manipulations in intrinsic chamber pressure (P_c) and longitudinal upstream (P_u) or downstream (P_d) gradients that can enlighten conditions under which collapse and narrowing result.

However, due to the uniformity of the elastic wall within the Starling resistor, such a model inadequately captures the impact of multiplane and multilevel forces on collapse, which is particularly relevant to adult OSA. Collapse is influenced by focal structural narrowing most commonly at retropalatal and retrolingual levels and can occur in concentric, anteroposterior (AP), or lateral axial planes, the combination of which results in different patterns of obstruction (Da Cunha Viana Jr et al., 2017). Benchtop models capable of replicating such complexity (particularly incorporating anatomical features of the pharyngeal wall) may considerably advance investigations on airflow characteristics and wall compliance and offer the possibility of patient-centric replicas for tailored treatments.

An ideal model would be easily produced based on dynamic airway examination and/or imaging data for an individual patient. Recent advances in medical 3D printing using biologically complementary materials now permits expedient and inexpensive manufacture of anatomically accurate models previously impossible to achieve (Schubert, Van Langeveld, & Donoso, 2014). In addition, the nonlinear complexity of interwoven rigid and malleable components working in tandem is producible and ideal for manipulating patterns of "airway" collapse to examine changes in airflow and buckling along a tube.

This study is the first to present results to that end, building an accurate benchtop model of the human upper airway in OSA. Furthermore, responsive magnetic iron and nickel-loaded polymers were implanted in the benchtop airway model design to investigate their use in reversal of airway narrowing.

2 | METHOD

2.1 | Overview and design

This study investigated the fluid dynamics of a benchtop model of the human upper airway in a multi factorial design:

- Firstly, the collapse pressure was investigated by varying the strut diameter of the airway.
- Secondly, the wall folding geometry was investigated through varying the geometrical design of the struts to produce either a representative AP collapse or a circumferential collapse.
- Lastly, a magnetic polymer was introduced to the airway to investigate the force required to change the pressure at which the airway collapsed.

2.2 | Airway modeling

The patient Magnetic Resonance Imaging DICOM (Digital Imaging and Communications in Medicine) files were uploaded into Materialise Mimics in order to digitally examine the area of interest. The airway was isolated by applying different masks; then, for completeness (and to investigate possible future personalized airway treatments), the 3D surface model of the upper airway's muscle was created as a 3D mask body (Figure 1). Examining the airway diameter at 10 intervals over a 50-mm length resulted in an average measured airway diameter of 12.57 mm. This representative airway cross-section diameter has been taken as the base value for our additively fabricated airway models.

2.3 | Printing airways

Airway representative models were produced in two steps via a customized pneumatic extrusion 3D printing system (KIMM SPS1000, M4T, Korea). This system includes a rotary axis (fourth Axis, denoted as A) which allowed for controlled rotation of the Ø12.57 mm mandrel below the extrusion tip outlet (Figure 2). The representative

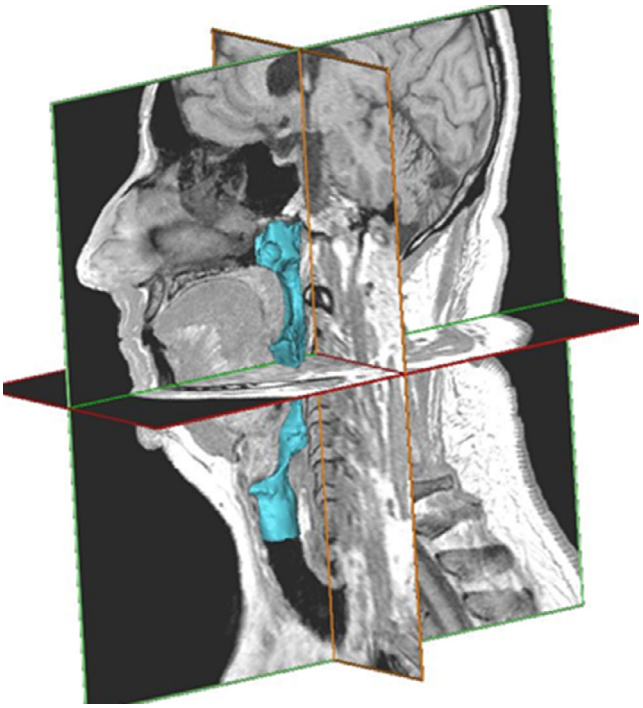

FIGURE 1 3D surface model of the upper airway's muscle was created as a 3D mask, using the Materialise Mimics Innovation Suite software

airways consist of two materials. First a controlled and sealed layer of an elastomeric UV curable tissue simulant (TangoPlus FLX930, Stratasys) was deposited. The flexible resin, kept at room temperature, was extruded through a 400-μm diameter metal nozzle fitted to a disposable syringe (Nordson EFD) at a feed rate of 100 mm/min with 15 kPa air pressure at a rotational speed of 100 degrees/s over a translation of 50 mm in the X translation direction. The printed resin was cross-linked by exposure to a 365-nm light source (Omnicure Series 1000).

Subsequently structural reinforcement elements (or struts), which resulted in different geometric features, were printed directly onto the pre-prepared elastomeric surface through hot melt extrusion printing of Polycaprolactone (MW 45000, Sigma Aldrich). This was achieved by interchanging of the resin extrusion head with a melt extrusion head (heating range: ambient—200°C) and pneumatically extruding the polymer reinforcement lines through a 400-μm stainless steel nozzle connected to a 316 stainless steel melt reservoir at a stable temperature of laboratory at a feed rate of 100 mm/min (Figure 3). To enable variation of the thickness of these reinforcement struts and in turn modulate the forces required to compress the trial airways, extrusion pressures of 400, 450, and 500 kPa were used and resulted in strut diameters of 0.8, 1.0, and 1.5 mm, respectively.

This two-step production process enabled the reproducible integration of geometric features to induce collapse at fixed regions within the airway. This allowed for the investigation of multiple collapse modes seen in sleep apnea patients to be generated and their effect on performance observed.

In order to prevent the collapse, printing process was repeated with the same settings and condition to print magnetic polymer composite as a structural lines instead of polycaprolactone. Magnetic composite was prepared by manually mixing 2 g of polycaprolactone with 2 g of iron powder (mean particle size 1–6 microns, Sigma Aldrich) over a hot plate at 80°C for 10 min.

2.4 | Fluid dynamics

The pressure flow relationships of the collapsible airways were studied by inserting the collapsible airways into a module that allowed the P_c around the airways to be increased to cause a collapse along with the ability to introduce a magnetic field (Figure 4).

The module was connected to a custom-built LabVIEW powered respiratory analysis system (Bibo, LabVIEWsoftware V6.1; National Instruments, Texas) supported by a fixed heated-pneumotachograph (Model 3813, Hans Rudolph Inc., Kansas) with attached pressure transducers (Validyne DP45/30 low differential pressure transducer, Engineering Corp., California; Figure 5). Pressure and flow signals were sampled at 50 Hz and digitized with a 16-bit 16 channel analog-to-digital converter (National Instruments DAQPad-6015). Airflow was generated via a vacuum source initially set at 200 ml/s, to

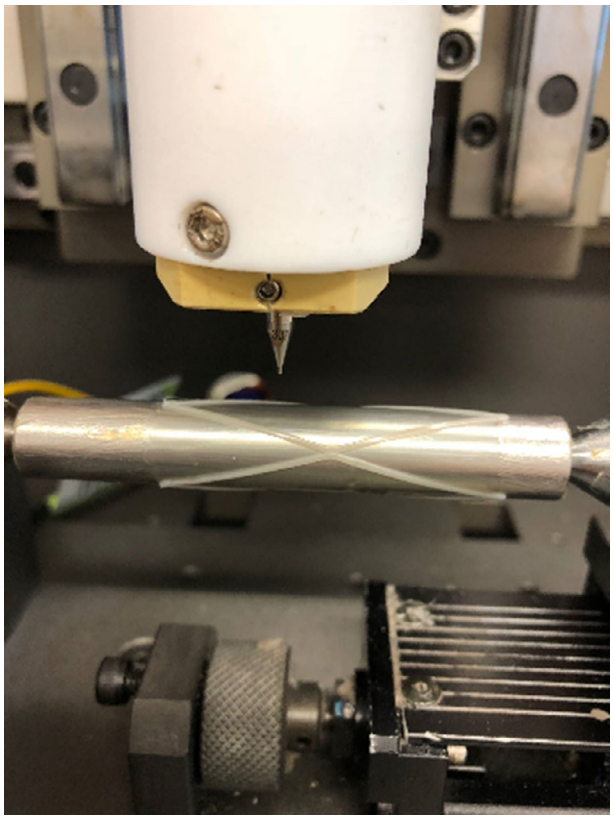

FIGURE 3 Structural lines as a second layer to create wall folding geometry: concentric and anteroposterior airway collapse

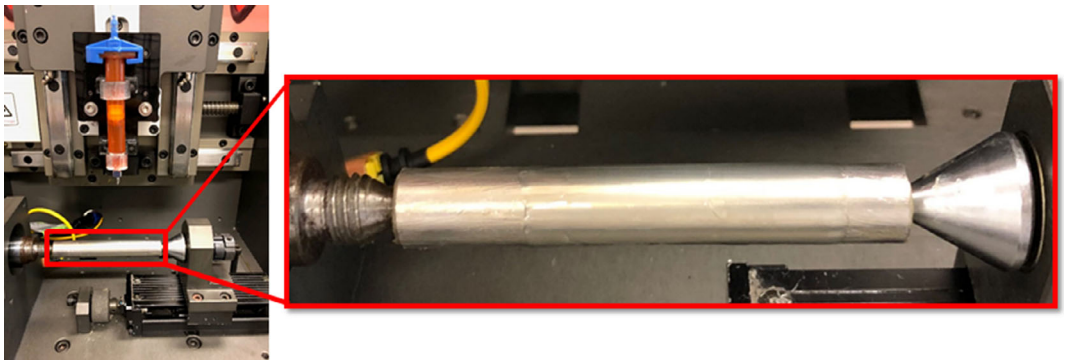

FIGURE 2 KIMM SPS1000 printer which is used for printing the upper airways

replicate mean airflow over a tidal volume that occurred during resting ventilation. Initial airflow ($V^{\cdot}_0$), P_c, intra airway differential/driving pressure (P_D), P_u—P_d, and tube lumen image were recorded. Measurements were taken in triplicate to ensure the airway collapse was reproducible at equivalent pressures.

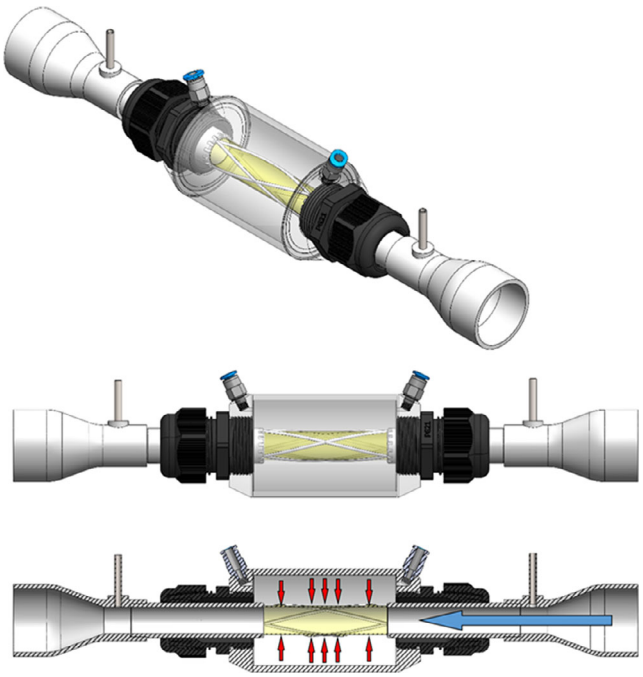

FIGURE 4 Airway support module

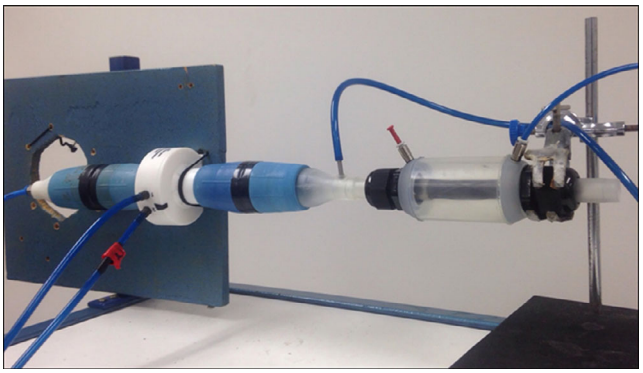

FIGURE 5 Model with pneumotachograph, pressure ports, and vacuum source

Injection or removal of air from the chamber was used to increase and decrease chamber pressure, respectively. The pressure flow relationship of the collapsible airways was measured via initially setting the airflow at 200 ml/s and increasing the chamber pressure until a flow reduction developed and recording the chamber pressure at the onset of flow reduction.

2.5 | Magnetic airway force production

The force produced by the interaction of the magnetic polymer and the magnetic module was studied by measuring a sample of the magnetic airways and the incoming force (cN) produced over varying distances using a force transducer by Shimadzu EZ-L universal mechanical tester.

3 | RESULTS

3.1 | Collapse pressure fluid dynamics

Increases in P_c resulted in reductions in the initial flow ($V^{\cdot}_0$ [200 ml/s]) in all collapsible printed airways. P_c at the onset of flow reduction ($P_{REDUCTION}$), the point of differential pressure inflection (P_D Inflection), and complete airway collapse ($P_{COLLAPSE}$), values were lowest for the airways with the lowest supporting strut diameter and increased with increasing strut diameter (0.8, 1.0–1.5 mm), collapse pressures ranged from 5.32 to 9.58 cmH_2O (Table 1 and Figures 6 and 7). This therefore demonstrates the ability to manipulate the pressure at which airway collapse occurs to match physiologically relevant pressures.

3.2 | Wall folding geometry fluid dynamics

Increases in P_c resulted in reductions in lumen cross-sectional area in all collapsible airways. Depending on the inbuilt structure of the printed airways, the geometry of the collapse was manipulated to represent either concentric or AP airway collapse (Figure 8). The 0.8-mm circumferential and 0.8-mm AP airways had similar $P_{REDUCTION}$, P_D Inflection, and $P_{COLLAPSE}$. Whereas the circumferential 1.0 and 1.5 mm airways required a greater pressure before $P_{REDUCTION}$, P_D Inflection, and $P_{COLLAPSE}$ (Table 1 and Figures 6 and 7). This therefore gives insight into the pressure changes that occur in different forms of sleep apnea airway collapse.

TABLE 1 Airway pressures for collapsible airways: Three face 0.8 mm, three face 1.0 mm, three face 1.5 mm, two face 0.8 mm, two face 1.0 mm, and two face 1.5 mm

Variable	Three face 0.8 mm	Three face 1.0 mm	Three face 1.5 mm	Two face 0.8 mm	Two face 1.0 mm	Two face 1.5 mm
$P_{COLLAPSE}$ (cmH_2O)	5.32	7.82	9.58	5.86	6.45	7.59
$P_{V^{\cdot}\ REDUCTION}$ (cmH_2O)	4.70	6.88	6.46	5.86	6.08	5.24
P_D Inflection (cmH_2O)	2.30	3.81	4.50	3.11	2.62	2.67

Abbreviations: $P_{COLLAPSE}$, chamber pressure at complete airway collapse; P_D Inflection, chamber pressure when P_D increases; $P_{V^{\cdot}\ REDUCTION}$, chamber pressure at onset of $V^{\cdot}$ reduction.

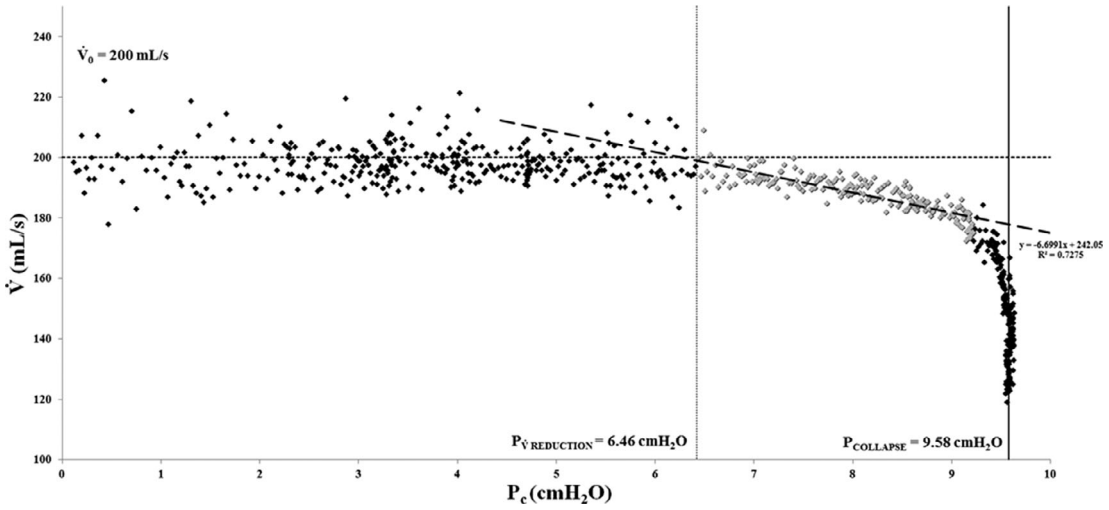

FIGURE 6 An example measure of chamber pressure (P_c) associated with onset of $\dot{V}$ reduction ($P_{REDUCTION}$) and complete airway collapse ($P_{COLLAPSE}$). Plot shows $\dot{V}$ vs P_c for baseline $\dot{V}$ ($\dot{V}_0$) = 200 ml/s (horizontal dotted line). Note the pressure of $\dot{V}$ reduction ($P_{REDUCTION}$; vertical dashed line), beyond which $\dot{V}$ linearly decreases with further increases in P_c, this is also illustrated by the diagonal dotted linear trend line; and the pressure of complete airway collapse ($P_{COLLAPSE}$; vertical solid line), where $\dot{V}$ is completely occluded

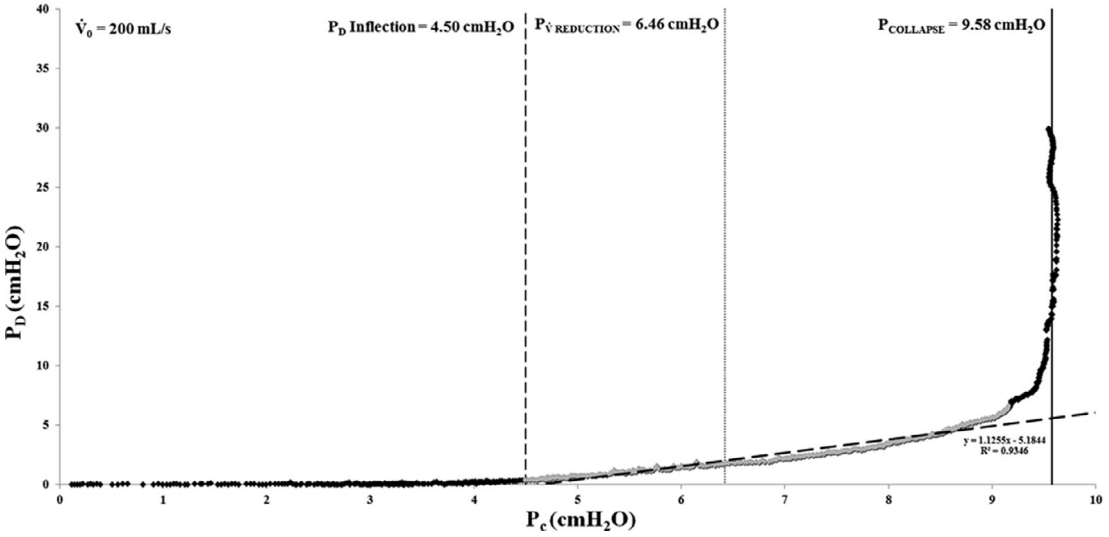

FIGURE 7 An example measure of chamber pressure (P_c) associated with P_D and complete airway collapse ($P_{COLLAPSE}$). Plot shows P_D vs P_c for baseline $\dot{V}$ ($\dot{V}_0$) = 200 ml/s. Note the pressure of P_D Inflection (P_D Inflection; vertical dashed line), beyond which P_D linearly increases with further increases in P_c, this is also illustrated by the diagonal dotted linear trend line; and the pressure of complete airway collapse ($P_{COLLAPSE}$; vertical solid line), where P_D increases exponentially and $\dot{V}$ is completely occluded

3.3 | Magnetic intervention fluid dynamics

The collapsible magnetically activated airways required far greater pressure before $P_{REDUCTION}$ and $P_{COLLAPSE}$ when the magnetic module was put in place. The iron polymer magnetically activated airway $P_{COLLAPSE}$ increased from 6.00 cmH$_2$O when not activated to 13.38 cmH$_2$O when activated. The nickel polymer magnetically activated airway $P_{COLLAPSE}$ increased by an even greater amount from 4.82 cmH$_2$O when not activated to 21.82 cmH$_2$O when activated. $P_{REDUCTION}$ and P_D Inflection values followed similar trends (Table 2). These increases in pressure before airway collapse might be physiologically significant if applied in a clinical setting. Such increases could possibly obliterate airway collapse by raising the threshold pressure for it to occur.

3.4 | Magnetic force production

The nickel and iron magnetically activated airways along with nickel and iron polymer samples were measured to investigate the force

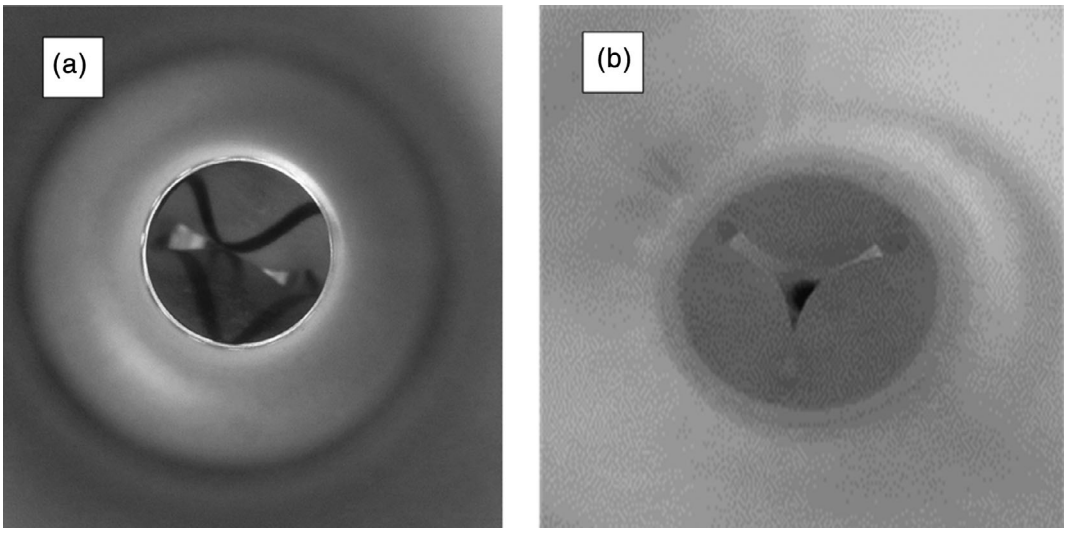

FIGURE 8 Wall folding geometry: concentric airway collapse (a) or anteroposterior airway collapse (b)

Variable	Two face 1.0 mm (Ni)		Two face 1.0 mm (Fe)	
	Magnetic	Nonmagnetic	Magnetic	Nonmagnetic
$P_{COLLAPSE}$ (cmH_2O)	21.82	4.31	13.38	6.00
$P_{V\cdot\ REDUCTION}$ (cmH_2O)	16.17	3.82	11.74	5.16
P_D Inflection (cmH_2O)	6.76	2.84	6.29	2.62

Abbreviations: $P_{COLLAPSE}$, chamber pressure at complete airway collapse; P_D Inflection, chamber pressure when P_D increases; $P_{V\cdot\ REDUCTION}$, chamber pressure at onset of $V^{\cdot}$ reduction.

TABLE 2 Airway pressures for collapsible airways with and without magnetic intervention: Two face 1.0 mm (nickel polymer) and two face 1.0 mm (iron polymer)

Variable	Fe sample	Ni sample	Two face 1.0 mm (Fe)	Two face 1.0 mm (Ni)
Peak force (cN)	81.59	163.34	48.59	72.04
Force distance (mm)	6.80	9.54	7.04	9.70

TABLE 3 Magnetic intervention force production: iron polymer sample, nickel polymer sample, two face 1.0 mm (nickel polymer) and two face 1.0 mm (iron polymer)

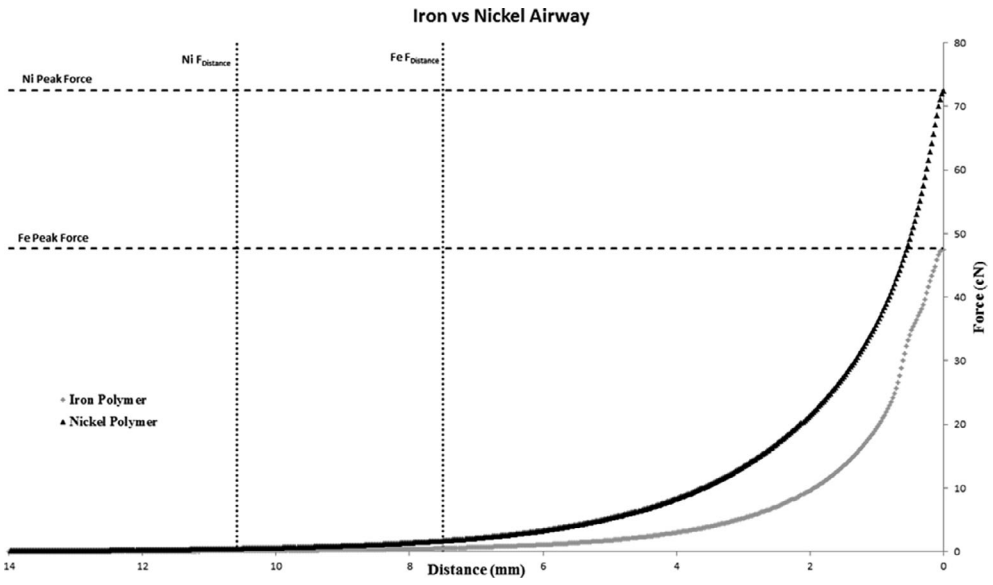

FIGURE 9 Magnetic intervention force production: two face 1.0 mm (nickel polymer) and two face 1.0 mm (iron polymer)

produced to hold the airway open and the distance at which the magnet interaction first produced force. The nickel polymer sample and magnetically activated airway produced a greater peak force (cN) and interacted with the magnet at a greater distance (mm) than the iron polymer sample and magnetically activated airway (Table 3 and Figure 9). This follows from the airflow characteristic of the airways with the nickel magnetically activated airway requiring higher forces than the iron magnetic activated airway to collapse. These force measurements may have future use in identifying polymer implantation to raise pressure thresholds required for airway collapse.

4 | DISCUSSION

Our objective was to 3D print an anatomically representative benchtop model of the adult human upper airway to produce multiplane levels of collapse known to occur in OSA at physiologically relevant pressures. Following this, responsive polymers were prepared and incorporated into the model airway structure to investigate their ability to withstand airway collapse at higher pressures. Development of three dimensional reconstructive geometries for the simulation of OSA can further extend the understanding of pharyngeal interactions, which challenge structural integrity during sleep. Individual airway architecture and elastic wall modulus combine to moderate flow and alter regions of patency as a mechanism to account for the heterogenous presentation of OSA.

Simple floppy tube starling resistors have previously been used to investigate upper airway collapse. It has been proposed that caudal traction displacements prevent airway collapse by increasing wall stiffness through increased longitudinal strain (Rowley, Permutt, Willey, Smith, & Schwartz, 1996). Manipulation of the strain on the collapsible tube shows changes in collapse geometry and airway pressure flow characteristics, giving insight into human upper airway collapse. The floppy tubes in previous starling resistor models, however, have been made completely uniform dissimilar to the human upper airway (Amatoury et al., 2010). By varying the strut diameter and position of struts within 3D printed airways, different severity and mechanisms of collapse were successfully investigated. The varying severity of the collapse points were physiologically relevant as the pressures of collapse were altered to match the passive pharyngeal critical closing pressure seen in both pathological and nonpathological individuals (Pcrit; Owens et al., 2012). This is a novel adaption of the starling resistor that allows for a more anatomically relevant representation of human upper airway collapse. Furthermore, due to the ability to minutely vary the characteristics of 3D printed airway designs, there is scope to create a model of specific patient airway collapse and personalize treatment relevant to the individual's condition.

The ultimate aim was to use the model to investigate the application of polymers to ameliorate OSA symptoms. This has been initially investigated using responsive magnetic polymers. Using iron and nickel composite polymers within the 3D printed airways and a magnetic module, the airways were investigated to measure their ability to withstand a greater chamber pressure before collapsing. The values obtained proved to be clinically relevant and if replicated in a pathological individual would prevent collapse and potentially ameliorate OSA symptoms. The force produced by magnetic polymers was investigated using a force transducer with the aim of using this information to inform the production of a responsive polymer surgical implant for use in future animal trials.

REFERENCES

Amatoury, J., Kairaitis, K., Wheatley, J. R., Bilston, L. E., & Amis, T. C. (2010). Onset of airflow limitation in a collapsible tube model: Impact of surrounding pressure, longitudinal strain, and wall folding geometry. *Journal of Applied Physiology*, *109*(5), 1467–1475.

Bilston, L. E., & Gandevia, S. C. (2013). Biomechanical properties of the human upper airway and their effect on its behavior during breathing and in obstructive sleep apnea. *Journal of Applied Physiology*, *116*(3), 314–324.

Brennick, M. J., Pack, A. L., Ko, K., Kim, E., Pickup, S., Masilin, G., & Schwab, R. J. (2009). Altered upper airway and soft tissue structires in the New Zealand obese mouse. *American Journal of Respiratory and Critical Care Medicine*, *179*, 158–169.

Brennick, M. J., Pickup, S., Cater, J. R., & Kuna, S. T. (2006). Phasic respiratory pharyngeal mechanics by magentic resonance imaging in lean and obese zucker rats. *American Journal of Respiratory and Critical Care Medicine*, *173*, 1031–1037.

Da Cunha Viana Jr, A., Mendes, D. L., de Andrade Lemes, L. N., Thuler, L. C. S., Neves, D. D., & de Araújo-Melo, M. H. (2017). Drug-induced sleep endoscopy in the obstructive sleep apnea: Comparison between NOHL and VOTE classifications. *European Archives of Oto-Rhino-Laryngology*, *274*(2), 627–635.

Hillman, D., Mitchell, S., Streatfeild, J., Burns, C., Bruck, D., & Pezzullo, L. (2018). The economic cost of inadequate sleep. *Sleep*, *41*(8), 1–13.

Huang, Y., Malhotra, A., & White, D. P. (2005). Computational simulation of human upper airway collapse using a pressure-/state-dependent model of genioglossal muscle contraction under laminar flow conditions. *Journal of Applied Physiology*, *99*(3), 1138–1148.

Owens, R. L., Edwards, B. A., Sands, S. A., Butler, J. P., Eckert, D. J., White, D. P., … Wellman, A. (2012). Upper airway collapsibility and patterns of flow limitation at constant end-expiratory lung volume. *Journal of Applied Physiology*, *113*(5), 691–699.

Rowley, J. A., Permutt, S., Willey, S., Smith, P. L., & Schwartz, A. R. (1996). Effect of tracheal and tongue displacement on upper airway airflow dynamics. *Journal of Applied Physiology*, *80*(6), 2171–2178.

Schubert, C., Van Langeveld, M. C., & Donoso, L. A. (2014). Innovations in 3D printing: A 3D overview from optics to organs. *British Journal of Ophthalmology*, *98*(2), 159–161.

Young, T., Palta, M., Dempsey, J., Skatrud, J., Weber, S., & Badr, S. (1993). The occurrence of sleep-disordered breathing among middle-aged adults. *The New England Journal of Medicine*, *328*, 1230–1235.

How to cite this article: Hingley L, Jeiranikhameneh A, Beirne S, et al. Modeling the upper airway: A precursor to personalized surgical interventions for the treatment of sleep apnea. *J Biomed Mater Res*. 2020;108A:1419–1425. https://doi.org/10.1002/jbm.a.36913